A cytosolic bifunctional geranyl/farnesyl diphosphate synthase provides MVA-derived GPP for geraniol biosynthesis in rose flowers

Corentin Conart, Dikki Pedenla Bomzan, Xing-Qi Huang, Jean-Etienne Bassard, Saretta N. Paramita, Denis Saint-Marcoux, Aurélie Rius-Bony, Gal Hivert, Anthony Anchisi, Hubert Schaller, et al.

PNAS RESEARCH ARTICLE | PLANT BIOLOGY

A cytosolic bifunctional geranyl/farnesyl diphosphate synthase provides MVA-derived GPP for geraniol biosynthesis in rose flowers

Corentin Conart[a], Dikki Pedenla Bomzan[a], Xing-Qi Huang[b], Jean-Etienne Bassard[c], Saretta N. Paramita[a], Denis Saint-Marcoux[a], Aurélie Rius-Bony[a], Gal Hivert[d,e], Anthony Anchisi[f], Hubert Schaller[c], Latifa Hamama[g], Jean-Louis Magnard[a], Agata Lipko[h], Ewa Swiezewska[i], Patrick Jame[f], Geneviève Riveill[j], Laurence Hibrand-Saint Oyant[g], Michel Rohmer[k], Efraim Lewinsohn[d,e], Natalia Dudareva[b,l,m], Sylvie Baudino[a], Jean-Claude Caissard[a], and Benoît Boachon[a,1]

Edited by Richard Dixon, University of North Texas, Denton, TX; received January 10, 2023; accepted March 30, 2023

Geraniol derived from essential oils of various plant species is widely used in the cosmetic and perfume industries. It is also an essential trait of the pleasant smell of rose flowers. In contrast to other monoterpenes which are produced in plastids via the methyl erythritol phosphate pathway, geraniol biosynthesis in roses relies on cytosolic NUDX1 hydrolase which dephosphorylates geranyl diphosphate (GPP). However, the metabolic origin of cytosolic GPP remains unknown. By feeding *Rosa chinensis* "Old Blush" flowers with pathway-specific precursors and inhibitors, combined with metabolic profiling and functional characterization of enzymes in vitro and in planta, we show that geraniol is synthesized through the cytosolic mevalonate (MVA) pathway by a bifunctional geranyl/farnesyl diphosphate synthase, RcG/FPPS1, producing both GPP and farnesyl diphosphate (FPP). The downregulation and overexpression of *RcG/FPPS1* in rose petals affected not only geraniol and germacrene D emissions but also dihydro-β-ionol, the latter due to metabolic cross talk of RcG/FPPS1-dependent isoprenoid intermediates trafficking from the cytosol to plastids. Phylogenetic analysis together with functional characterization of G/FPPS orthologs revealed that the G/FPPS activity is conserved among *Rosaceae* species. Site-directed mutagenesis and molecular dynamic simulations enabled to identify two conserved amino acids that evolved from ancestral FPPSs and contribute to GPP/FPP product specificity. Overall, this study elucidates the origin of the cytosolic GPP for NUDX1-dependent geraniol production, provides insights into the emergence of the RcG/FPPS1 GPPS activity from the ancestral FPPSs, and shows that RcG/FPPS1 plays a key role in the biosynthesis of volatile terpenoid compounds in rose flowers.

rose | geraniol | GPP | FPP | *Rosaceae*

Roses are known for centuries for their pleasant characteristic fragrance and esthetic morphological traits appealing to humans. Despite the wide diversity of volatile organic compounds (VOCs) emitted by thousands of rose hybrids created so far, geraniol and its derivatives such as citronellol are essential compounds contributing to unique and familiar rose scents (1). Unlike other monoterpenes, the carbon skeleton of geraniol is identical to its precursor geranyl diphosphate (GPP). This structural feature initially allowed to hypothesize that geraniol could be formed by the action of a phosphatase. However, the characterization of the first geraniol synthase enzyme (GES) from sweet basil (2) revealed that geraniol biosynthesis involves, like in the case of other monoterpene synthases, the formation of a carbocation intermediate from GPP substrate in plastids. Since then, this canonical geraniol biosynthetic pathway was described in most geraniol-producing plants, except for roses. Instead of a plastidic GES, a cytosolic RhNUDX1 hydrolase was recently shown to be responsible for the production of geraniol in flowers of rose hybrids (3). NUDX hydrolases are conserved enzymes found in all types of organisms and are considered as "housecleaning" proteins associated with cell detoxification such as the dephosphorylation of organic diphosphates (4). However, in rose hybrids and wild species producing geraniol, *NUDX1-1a* is highly and specifically expressed in petals and its encoding protein dephosphorylates cytosol-localized GPP to geranyl monophosphate, an intermediate in the geraniol biosynthesis (5). GPP is generally assumed to be synthesized in plastids, from five-carbon building blocks, isopentenyl diphosphate (IPP), and its allylic isomer dimethylallyl diphosphate (DMAPP) derived from the methyl-erythritol 4-phosphate (MEP) pathway. The fact that the rose NUDX1-1a is localized exclusively in the cytosol, and not in plastids, raised yet the unanswered question about the origin of GPP metabolized by cytosolic NUDX1-1a in roses.

Significance

Geraniol, a volatile compound contributing to the unique smell of rose flowers, is synthesized through a noncanonical NUDX1-dependent pathway from cytosolic geranyl diphosphate (GPP), the origin of which remained unknown. We demonstrate that in contrast to the heterodimeric GPP synthase providing plastidic GPP in most plants, a cytosolic and bifunctional FPP synthase enzyme produces both GPP and farnesyl diphosphate (FPP) via the mevalonate pathway in rose flowers. This enzyme, conserved in *Rosaceae* species, evolved from ancestral FPPSs with two amino acids contributing to GPP/FPP product specificity. It plays a key role in the emission of geraniol and also germacrene D and dihydro-β-ionol, the latter is due to trafficking of RcG/FPPS1-dependent isoprenoid intermediates from the cytosol to plastids.

Author contributions: C.C., X.-Q.H., G.H., E.S., P.J., L.H.-S.O., M.R., E.L., N.D., S.B., J.-C.C., and B.B. designed research; C.C., D.P.B., X.-Q.H., J.-E.B., S.N.P., A.R.-B., G.H., A.A., H.S., L.H., J.-L.M., A.L., G.R., and B.B. performed research; C.C., D.P.B., X.-Q.H., J.-E.B., S.N.P., D.S.-M, P.J., and B.B. analyzed data; and C.C., X.-Q.H., N.D., S.B., J.C.-C., and B.B. wrote the paper.

The authors declare no competing interest.

This article is a PNAS Direct Submission.

[1]To whom correspondence may be addressed. Email: benoit.boachon@univ-st-etienne.fr.

This article contains supporting information online at https://www.pnas.org/lookup/suppl/doi:10.1073/pnas.2221440120/-/DCSupplemental.

Published May 1, 2023.

In plants, IPP and DMAPP are synthesized by two alternative and compartmentally separated pathways: the plastidic MEP pathway and the MVA pathway distributed between the cytosol, endoplasmic reticulum, and peroxisomes (6, 7). These two pathways are connected via a metabolic "cross talk," which is species- and organ-specific (8). Both IPP and DMAPP are substrates for short-chain *trans*-isopentenyl-diphosphate synthases (IDSs), which produce prenyl diphosphate precursors, GPP, farnesyl diphosphate (FPP), and geranylgeranyl diphosphate (GGPP). In general, FPP synthases (FPPSs) use the MVA-derived IPP and DMAPP to produce FPP for cytosolic biosynthesis of sesquiterpenes and triterpenes and mitochondrial biosynthesis of ubiquinones. GPP synthases (GPPSs) and GGPP synthases (GGPPs) utilize the MEP-derived IPP and DMAPP to form GPP and GGPP, respectively, which are generally used for the formation of monoterpenes, diterpenes, and tetraterpenes such as carotenoids in plastids. In addition, several studies reported that GGPP and diterpenes can be synthesized in the cytosol (9–11). In contrast, for a long time, it was accepted that the biosynthesis of GPP occurs in plastids except for *Lithospermum erythrorhizon* roots in which shikonin production was known to rely on cytosolic GPPS activity (12, 13). However, over the last decades, numerous studies showed that the biosynthesis of monoterpenes can also occur in the cytosol (14–20), suggesting the existence of a cytosolic GPP pool in plants for which the biosynthetic origin remained unknown. This raised the question of how plants produce GPP in the cytosol and how widespread is this phenomenon in the plant kingdom.

All plant IDSs are homodimeric enzymes except for GPPSs (21), which have both homodimeric and heterodimeric architectures depending on plant species. The homodimeric GPPSs have been described in gymnosperm and some angiosperm species (22–26), while the heteromeric GPPSs have been reported only in angiosperms so far including *Arabidopsis thaliana*, *Mentha piperita*, *Solanum lycopersicum*, *Antirrhinum majus, Catharanthus roseus,* and *Humulus lupulus* (23, 27–31). The heterodimeric GPPSs consist of a large subunit (LSU), usually exhibiting GGPPS activity alone, and a small subunit (SSU), which is generally catalytically inactive but upon interaction with the large subunit, favors GPP formation. In addition, a cytosolic homodimeric GPPS with similarity to FPPSs was recently characterized from *L. erythrorhizon* (32, 33). Thus, the cytosolic GPP in plants could derive from products of the MVA, the MEP pathway, or both due to the existence of cross talk between the two terpenoid biosynthetic pathways via the exchange of IPP and GPP (34) and rely either on homodimeric or heterodimeric GPPSs or on FPPS-like enzymes producing GPP.

In this study, we used *Rosa chinensis* "Old Blush" flowers (RcOB) (35, 36) to investigate the origin of cytosolic GPP utilized by NUDX1-1a to produce high level of geraniol. We demonstrated that GPP is synthesized in the cytosol via the MVA pathway. Biochemical characterization of five IDS candidates retrieved from RcOB genome revealed that one cytosolic FPPS-like enzyme, named RcG/FPPS1 (geranyl/farnesyl diphosphate synthase), exhibits both GPPS and FPPS activities in vitro. Coexpression of the five IDS candidates with *RcNUDX1-1a* in *Nicotiana benthamiana* leaves showed that only *RcG/FPPS1* enabled increased geraniol production, although its expression alone increased FPP-derived capsidiol accumulation. In addition, *RcG/FPPS1* transcript levels in rose flowers exhibited a rhythmic profile that correlated with both GPP and FPP accumulations and preceded geraniol emission. Transient down- and up-regulation of *RcG/FPPS1* expression in rose flowers resulted in respective decrease and increase of geraniol emission. A similar effect was also observed on emissions of FPP-derived germacrene D and carotenoid-derived dihydro-β-ionol (dhβ-ionol), thus providing genetic evidence for RcG/FPPS1 bifunctional activity in planta and its major role in the biosynthesis of terpenoid VOCs including geraniol in rose flowers.

Results

Geraniol Is Synthesized via the MVA Pathway in Rose Flowers. To investigate the biosynthetic origin of cytosolic GPP utilized by RcNUDX1-1a for geraniol production in rose flowers, several independent approaches were used including i) feeding flowers with stable isotope-labeled pathway-specific precursors, ii) inhibition experiments with pathway-specific inhibitors, iii) and assessment of subcellular localization of GPPS activity. Experiments were performed on RcOB flowers at anthesis (day 1) from stage 4 to 6 as depicted in Fig. 1 *A* and *B*. To determine the contribution of the MVA and/or MEP pathways to the cytosolic GPP formation, RcOB flowers were fed with (2-^{13}C)-mevalonolactone (^{13}C-MVL) and 1-deoxy-(5,5-$^{2}H_2$)-D-xylulose ($^{2}H_2$-DX), specific precursors of the MVA and MEP pathways, respectively (Fig. 1*C*). ^{13}C-MVL rapidly incorporated in geraniol and germacrene D, with the latter used as a marker of the MVA pathway since it is known to be produced from FPP by the cytosolic germacrene D synthase (GDS) (37) resulting in 42% and 64% labeling after 54 h of feeding, respectively. In contrast, feeding with $^{2}H_2$-DX led to relatively low and slow labeling of these compounds. Both precursors slowly incorporated in dhβ-ionol, an apocarotenoid VOC synthesized from plastidic GGPP (38), resulting in only 13% labeling for ^{13}C-MVL and 21% labelling for $^{2}H_2$-DX after 54 h of feeding (Fig. 1*C*). Consistent with these data, treatment of rose flowers with mevinolin, a specific inhibitor of the MVA pathway, decreased geraniol emission by 68%, which was similar to a reduction in emission of germacrene D (73%; Fig. 1*D*). On the contrary, fosmidomycin, a specific inhibitor of the MEP pathway, did not affect the emission of these compounds, suggesting that the cytosolic MVA pathway makes a major contribution to geraniol biosynthesis in rose flowers. In contrast, both inhibitors reduced the emission of dhβ-ionol, suggesting that both MVA and MEP pathways contribute to its formation and that a substantial export of isoprenoid intermediates from the cytosol to plastids occurs in rose flowers. The emission of 1,3,5-trimethoxybenzene (TMB), a nonterpene VOC produced from acetyl-CoA independently of the MEP and MVA pathways (39), was used as a control and remained unchanged in these experiments. Finally, subcellular localizations of GPPS and FPPS activities were analyzed, since GPPSs in most angiosperm species are localized in plastids, but our inhibition and feeding experiments suggested that the cytosolic MVA pathway predominantly contributes to geraniol formation in rose flowers. Both GPPS and FPPS activities were mainly detected in the cytosolic fraction, suggesting that GPP formation takes place in the cytosol in rose petals (Fig. 1*E*). Analysis of the activities of marker enzymes and chlorophyll content confirmed that the cytosolic fraction was barely contaminated by the other organelles (*SI Appendix*, Table S1). In contrast, plastidic and mitochondrial fractions contained negligible GPPS and FPPS activities relative to the cytosol. GGPPS activity was not detected in these experiments because of being below the detection limit. Taken together, these results suggest that in rose flowers, GPP is formed in the cytosol by unknown GPPS synthase from precursors derived from the MVA pathway.

The Cytosolic RcG/FPPS1 Exhibits Both GPP and FPP Synthase Activities. To identify the enzyme responsible for cytosolic GPP production in roses, we tBLASTn-searched the recently published RcOB genome (35, 36) for genes encoding *trans*-short-chain IDSs. This analysis revealed six IDS candidates including two putative FPPSs named RcG/FPPS1 (see below) and RcFPPS2, two

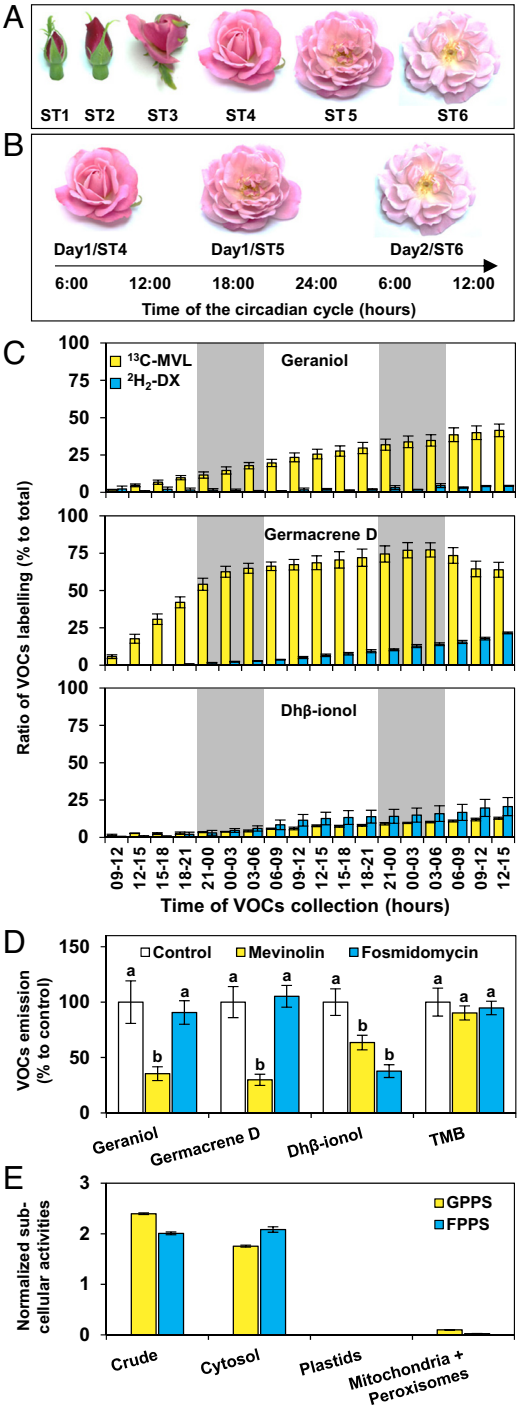

Fig. 1. Geraniol is synthesized through the MVA pathway in the cytosol of rose flower petals. (*A*) Pictures showing the six developmental stages (ST) of RcOB flowers (ST1 to 6) used in this study. (*B*) Pictures and diagram showing the development stages of flowers and the times of collection used in this study. Day1 corresponds to the day of anthesis. (*C*) Kinetic of stable isotopes ^{13}C-MVL [(2-^{13}C)-mevalonolactone] or $^{2}H_2$-DX (1-deoxy-(5,5-$^{2}H_2$)-D-xylulose) incorporation in VOCs emitted from RcOB flowers analyzed by GC-MS and expressed as % relative to total, mean ± SEM, n = 4. (*D*) Effect of inhibitor treatments of mevinolin or fosmidomycin on VOCs emitted from RcOB flowers analyzed by GC-MS and expressed as % relative to untreated control flowers. Data are means ± SEM, n = 18. Letters indicate statistically significant differences between samples analyzed by ANOVA and Tukey post-hoc test. (*E*) Subcellular GPPS and FPPS activities in crude protein extracts from RcOB flower petals and enriched organelles with cytosolic, plastidic, and mitochondrial/peroxisomal fractions. Proteins (20 µg per fraction) were incubated with IPP and DMAPP (10 µM). Methanolic extracts of products were analyzed by LC-MS/MS. Specific activities are expressed in pKat.mg^{-1} proteins normalized by the ratio of proteins recovered from each compartment compared to crude. Data are means ± SEM, n = 3.

putative large subunits of G(G)PPS designated RcGGPPS.LSU1 and RcGGPPS.LSU2, one small subunit of GPPS designated RcGPPS.SSU, and one putative homodimeric GPPS designated RcGPPS.HOMO (Fig. 2*A*), all containing the expected conserved domains typical for these IDS subfamilies (*SI Appendix*, Fig. S1). RNA-Seq analysis of flowers from RcOB and nine cultivars of *Rosa x hybrida* producing different levels of geraniol revealed transcripts for all identified candidates except for *RcGGPPS.LSU2*, which was then excluded from further analysis (Fig. 2*B*). The expression of the five *IDSs* was relatively low compared to *RcNUDX1-1a* and none of them was correlated with geraniol levels contrarily to *RcNUDX1-1a* expression. A protein targeting prediction program, TargetP, revealed no organellar-specific transit peptides only in RcG/FPPS1 and RcFPPS2, which are likely localized in the cytosol, in contrast to the small and large subunits of GPPS containing putative plastidic transit peptides and RcGPPS.HOMO possessing a putative mitochondrial transit peptide (*SI Appendix*, Fig. S1*A*). To verify the program predictions, the coding sequence (CDS) of each IDS candidate was fused to the N terminus of the CDS of the enhanced green fluorescent protein (eGFP) reporter for transient expression in RcOB petals. The observed subcellular localization in conical epidermal cells of RcOB petals was consistent with the program predictions (Fig. 2*C* and *SI Appendix*, Fig. S1*A*). Both RcG/FPPS1 and RcFPPS2 were localized in the cytosol like RcNUDX1-1a, while RcGPPS.SSU and RcGGPPS.LSU1 were colocalized with the plastidic marker as well as with each other and RcGPPS.HOMO was colocalized with the mitochondrial marker.

To determine whether identified cytosol-localized candidates can produce GPP, recombinant RcG/FPPS1 and RcFPPS2 proteins were heterologously produced in *Escherichia coli.* Purified proteins were incubated with IPP and DMAPP followed by LC-MS/MS product analysis (Fig. 3*A* and *SI Appendix*, Fig. S2*A*). Surprisingly, RcG/FPPS1 efficiently converted IPP and DMAPP substrates into both GPP and FPP, while RcFPPS2 almost exclusively produced FPP. When both enzymes were incubated with IPP and GPP, FPP was formed (*SI Appendix*, Fig. S2*B*). In addition, the GPP/FPP product ratio of RcG/FPPS1 could be modified by changing the ratio of supplied IPP and DMAPP substrates, producing more GPP in the presence of an excess of DMAPP and more FPP when IPP was provided in excess (Fig. 3*B*). Analysis of the kinetic parameters for GPP production revealed that RcG/FPPS1 had a high affinity toward IPP in the presence of DMAPP with an apparent K_m of 0.44 µM (Table 1). An apparent K_m of RcFPPS2 for GPP production could not be determined because it was fast converted to FPP. However, when kinetic parameters were determined for FPP production in the presence of GPP as allylic cosubstrate, RcG/FPPS1 had a fourfold lower affinity for IPP than that of RcFPPS2. Moreover, the RcG/FPPS1 affinity for IPP was 120-fold lower when GPP was supplied instead of DMAPP as cosubstrate and RcG/FPPS1 produced FPP 15-fold less efficiently (k_{cat}/K_m ratio) than that of GPP. Thus, RcG/FPPS1 gained the ability to produce GPP while keeping similar catalytic efficiency for FPP production as RcFPPS2, suggesting that RcG/FPPS1 is a bifunctional G/FPPS whose product specificity can be modified by substrate availability.

To test whether the other isolated candidates, RcGGPPS.LSU1, RcGPPS.SSU, and RcGPPS.HOMO, could also produce GPP, their corresponding recombinant proteins were analyzed. The identification of RcGPPS.SSU suggested that rose petals might contain a heterodimeric GPPS. Copurification of 6-His-tagged RcGGPPS.LSU1 with untagged RcGPPS.SSU resulted in heterodimeric protein (*SI Appendix*, Fig. S3*A*), product specificity of which as well as the small and large subunits alone and RcGPPS.

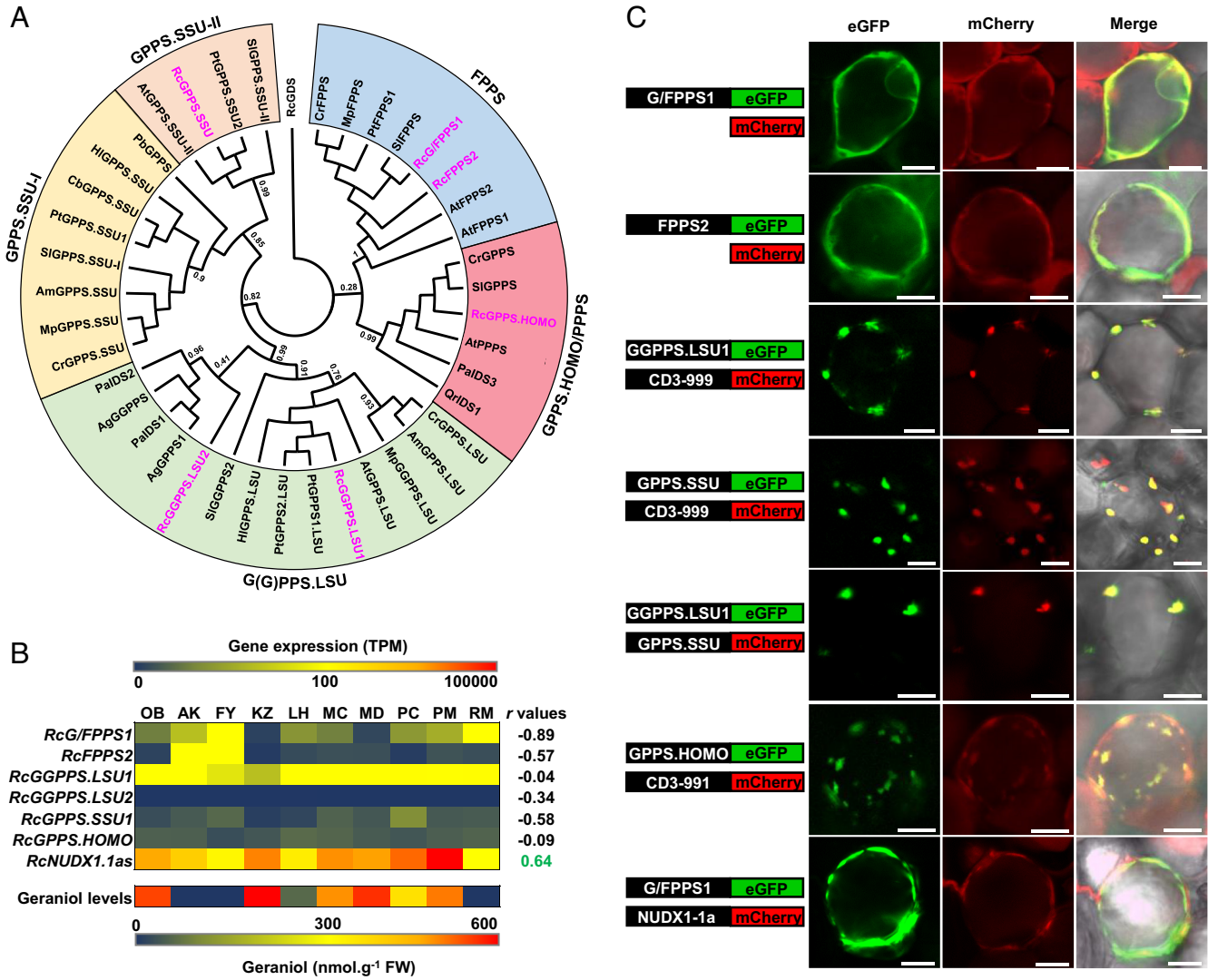

Fig. 2. The RcOB genome contains six IDS candidates of which two FPPS-like synthases localized in the cytosol. (*A*) Maximum likelihood tree of protein sequences of the six RcOB *trans*-short-chain IDSs (highlighted in pink) with characterized IDSs from *Abies grandis* (Ag), *Antirrhinum majus* (Am), *Arabidopsis thaliana* (At), *Clarkia breweri* (Cb), *Catharanthus roseus* (Cr), *Humulus lupulus* (Hl), *Mentha piperita* (Mp), *Phalaenopsis bellina* (Pb), *Picea abies* (Pa), *Populus trichocarpa* (Pt), *Quercus robur* (Qr), *Rosa chinensis* "Old Blush" (Rc), and *Solanum lycopersicum* (Sl). Numbers correspond to bootstrap values. Tree is rooted on RcGDS (Germacrene D synthase). Polyprenyl pyrophosphate synthase (PPPS). (*B*) Transcriptomic analysis of the six RcOB *IDSs* and *RcNUDX1-1as* compared to geraniol levels in *R. chinensis* "Old Blush" (OB) and 9 *Rosa x hybrida* cultivars including *R.* x *hybrida* "Akito" (AK), *R.* x *hybrida* "The Fairy" (FY), *R.* x *damascena* "Kazanlik" (KZ), *R.* x *odorata* "Lady Hillingdon" (LH), *R.* x *hybrida* "The Mc Cartney rose" (MC), *R.* x *hybrida* "Marius Ducher" (MD), *R.* x *hybrida* "Pariser Charme" (PC), *R.* x *hybrida* "Papa Meilland," (PM) and *R.* x *hybrida* "Rouge Meilland" (RM). Heatmap on top panel shows the expression levels of the six *IDS* candidates and *RcNUDX1-1as* from RNA-Seq analysis on open flowers (Stage 5) from the 10 rose cultivars and expressed as transcripts per million (TPM). Data are means from three biological replicates. Expression level for *RcNUDX1-1as* represents the sum of TPMs of the five *RcNUDX1-1as* present in the RcOB genome (7). Heatmap on bottom panel shows the geraniol levels analyzed in the flowers (Stage 5) of these 10 cultivars. Data are means from two to seven biological replicates. Pearson's *r* correlation coefficients comparing the transcript levels of each gene to geraniol content in the 10 rose cultivars are shown on the right of top panel. *r* values with significant *P* values (≤0.05) are highlighted in green. (*C*) Subcellular localization of RcOB IDSs in conical epidermal cells of RcOB petals. Schematic diagrams of the constructs used are shown on the left with corresponding transient expression in RcOB cells on the right. CDS of RcOB *IDS* candidates and *RcNUDX1-1a* were fused with eGFP or mCherry at their C terminus as indicated**.** mCherry was fused to different subcellular markers for cytosol (untargeted mCherry), plastids (CD3-999), and mitochondria (CD3-991). Merge channel shows both eGFP and mCherry signals with bright field (Scale bar, 10 μm.).

HOMO was analyzed (Fig. 3*A* and *SI Appendix*, Fig. S2). In the presence of IPP and DMAPP, GPP production was found for all the analyzed IDS candidates. However, it was less efficient than that by RcG/FPPS1 and never as a final product. To assess the end product formed by each IDS, the enzymes were incubated with GPP or FPP in the presence of IPP (*SI Appendix*, Fig. S2 *B* and *C*). FPP was the final product of RcGPPS.HOMO and RcGPPS.SSU, an unexpected activity of the latter is likely due to the presence of an alternative SARM motif (*SI Appendix*, Fig. S1). RcGGPPS.LSU1 produced GGPP as a final product and its coexpression with RcGPPS.SSU led only to a slight decrease in GGPP production with a simultaneous small increase in GPP level (*SI Appendix*, Fig. S2 *A–C*), suggesting that the heterodimeric GPPS in rose is not efficient in producing GPP as a sole product. Kinetic characterization of recombinant proteins for GPP production revealed that their apparent K_m for IPP ranged from 2.50 to 6.74 μM (Table 1). Out of four proteins, the heterodimeric GPPS had the highest affinity toward IPP in the presence of both DMAPP and catalytic efficiency, which were respectively 5.7-fold and 81-fold lower than that of RcG/FPPS1 (Table 1). Thus, these results show that out of all characterized candidates, the bifunctional RcG/FPPS1 is the most efficient enzyme producing GPP and based on its subcellular localization is likely responsible for cytosolic GPP formation in rose petals.

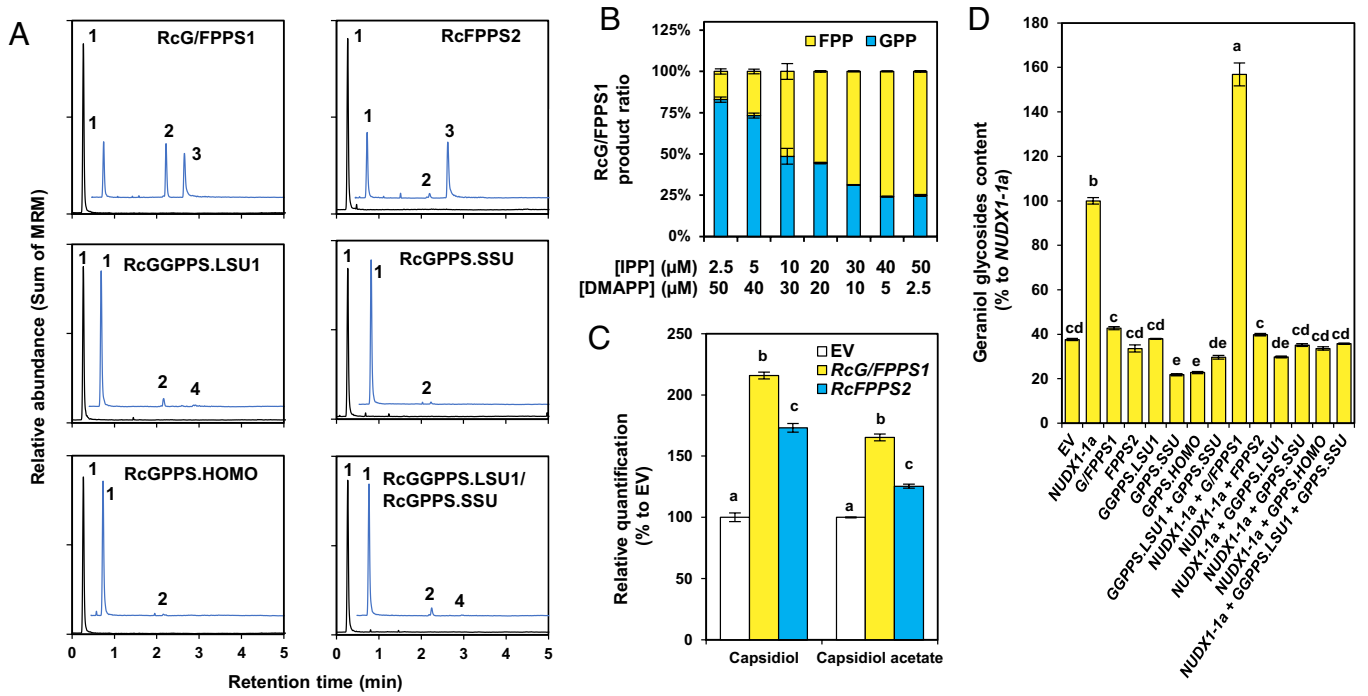

Fig. 3. RcG/FPPS1 is a bifunctional enzyme producing GPPS and FPPS in vitro and in planta. (*A*) LC-MS/MS chromatograms of the reaction products from in vitro incubation of the five RcOB IDS candidates and the heterodimeric GPPS (RcGGPPS.LSU1/RcGPPS.SSU) with IPP and DMAPP. Chromatograms in blue represent the incubation of 250 ng of each protein for 5 min with 10 μM IPP and DMAPP substrates at 30 °C. Chromatograms in black represent the negative controls with incubation of the corresponding boiled proteins. 1 = DMAPP + IPP, 2 = GPP, 3 = FPP, 4 = GGPP. (*B*) LC-MS/MS quantification of the RcG/FPPS1 GPP/FPP product ratio depending on the indicated concentrations of IPP and DMAPP provided. Incubations were realized as described in *A*. Data are means ± SEM, n = 3. (*C*) GC-MS quantification of the FPP-derived capsidiol and capsidiol acetate accumulating in *Nicotiana benthamiana* leaves transiently expressing empty vector (EV), *RcG/FPPS1*, or *RcFPPS2* alone. Data are relative quantification to EV set at 100 %, mean ± SEM, n = 3. Letters depict statistically significant differences analyzed by ANOVA and Tukey post-hoc test. (*D*) LC-MS/MS quantification of geraniol glycosides extracted from *N. benthamiana* leaves transiently expressing the five RcOB *IDS* candidates and the heterodimeric GPPS (*RcGGPPS.LSU1/RcGPPS.SSU*) alone or in coexpression with *RcNUDX1-1a*. Data are relative quantification to *NUDX1-1a* set at 100 %, mean ± SEM, n = 4. Letters depict statistically significant differences analyzed by ANOVA and Tukey post-hoc test.

To test whether RcG/FPPS1 displays both GPPS and FPPS activities in planta, *RcG/FPPS1* was transiently expressed in *N. benthamiana* leaves and compared with *RcFPPS2* expression used as a control for FPPS activity. Transient expression of both genes resulted in increased accumulation of capsidiol and capsidiol acetate (Fig. 3*C*), two FPP-derived sesquiterpenes known to accumulate in tobacco leaves (40), confirming that RcG/FPPS1 indeed exhibits FPPS activity in planta. Previously, it was reported that *N. benthamiana* leaves produced geraniol glycosides and *RcNUDX1-1a* overexpression increased their levels (3). Coexpression of *RcNUDX1-1a* only with *RcG/FPPS1* and not any of the other IDS candidates further increased geraniol glycoside levels when compared to *RcNUDX1-1a* expression alone (Fig. 3*D*), supporting that RcG/FPPS1, in addition to FPPS activity, also exhibits GPPS activity in planta. Overall, these results provide biochemical and genetic evidence that the cytosolic RcG/FPPS1 is a bifunctional enzyme capable of producing cytosolic FPP and GPP in planta.

RcG/FPPS1 Rhythmic Expression Precedes Rhythmic GPP and FPP Production. To further investigate the role of *RcG/FPPS1* for geraniol production in RcOB flowers, we analyzed RNA-Seq datasets generated from petals over six flower development stages starting from closed buds to fully opened flowers and at two time points during a day/night cycle (12:00 h and 24:00 h) (as depicted in Fig. 1 *A* and *B*). All identified *IDS*s exhibited very low expression levels compared to *RcNUDX1-1a* (*SI Appendix*, Fig. S4*A*), which

Table 1. Kinetic parameters of RcOB IDS candidates and RcG/FPPS1 mutants

Substrates		Product	Protein	Apparent K_m (μM)	k_{cat} (s^{-1})	k_{cat}/K_m $\mu M^{-1}.s^{-1}$)
DMAPP (60 μM)	Δ IPP (0.5–50 μM)	GPP	RcG/FPPS1	0.44 ± 0.03	0.321 ± 0.009	0.74 ± 0.03
			RcGGPPS.LSU1 + RcGPPS.SSU	2.50 ± 0.15	0.023 ± 0.0008	0.0091 ± 0.0003
			RcGGPPS.LSU1	6.74 ± 0.84	0.021 ± 0.002	0.0032 ± 0.0001
			RcGPPS.HOMO	5.00 ± 1.29	0.001 ± 0.0001	0.0001 ± 0.00001
			FPPS2	ND	ND	ND
GPP (60 μM)	Δ IPP (0.5–50 μM)	FPP	RcG/FPPS1	53.1 ± 5.1	2.87 ± 0.26	0.05 ± 0.000
			RcFPPS2	13.1 ± 3.4	0.91 ± 0.17	0.07 ± 0.006
			RcG/FPPS1-F88Y	9.08 ± 0.74	0.54 ± 0.03	0.06 ± 0.002
			RcG/FPPS1-V123I	14.74 ±1.94	0.93 ± 0.08	0.06 ± 0.003
			RcG/FPPS1-F88Y/V123I	12.78 ± 3.07	1.78 ± 0.33	0.14 ± 0.011

All values represent mean ± SE, n = 3. ND, not determined (below detection limit). Δ indicates the variable substrate.

was confirmed by RT-qPCR analysis with gene-specific primers (*SI Appendix*, Fig. S4 *B* and *C*). In addition, transcript levels of none of them correlated with geraniol emission (*SI Appendix*, Fig. S4*A*). In contrast, *RcNUDX1-1a*, *RcHMGRs,* and *RcHDR*, genes known to encode proteins catalyzing rate-limiting steps in the geraniol, the MVA, and the MEP biosynthetic pathways, respectively, displayed a statistically significant positive correlation with geraniol emission (*SI Appendix*, Fig. S4*A*). In addition, RNA-Seq analysis showed that *RcG/FPPS1* was higher expressed at night (24:00 h) than during day (12:00 h) (*SI Appendix*, Fig. S4*A*). Thus, a detailed analysis of expression of all *IDS*s was performed by RT-qPCR over a daily light/dark cycle, which revealed that only *RcG/FPPS1* exhibits a strong rhythmic expression pattern with a maximum expression at night (Fig. 4*A* and *SI Appendix*, Fig. S4*C*). Outstandingly, this rhythmic expression correlated with the peaks of both rhythmic GPP and FPP accumulation inside petal tissues (Fig. 4*B*) and ultimately geraniol emission (Fig. 4*C*) with the peak of each step (*RcG/FPPS1* expression -> GPP and FPP accumulation -> geraniol emission) preceding the following one by 3 to 6 h (Fig. 4 *A*–*C*). Germacrene D and dhβ-ionol displayed relatively similar rhythmic emission pattern (Fig. 4*C*). These results further support that *RcG/FPPS1* contributes to GPP and FPP formation in rose petals and ultimately to their derived VOC products.

RcG/FPPS1 Is Involved in Geraniol, Germacrene D, and dhβ-Ionol Biosynthesis in Planta. To examine the in vivo function of RcG/FPPS1, expression of the corresponding gene was transiently RNAi down-regulated in RcOB flowers. A 50% reduction in *RcG/FPPS1* transcript levels (Fig. 4*D*) led to a 57% decrease in geraniol emission relative to the EV control (Fig. 4*E*), providing strong genetic evidence that RcG/FPPS1 is responsible for the formation of cytosolic GPP and subsequently geraniol in roses. Emission of germacrene D, biosynthesis of which relies on FPP substrate, was also reduced by 30%, suggesting that RcG/FPPS1 acts as a bifunctional enzyme in planta that possesses both FPPS and GPPS activities. In addition, there was a 47% reduction in dhβ-ionol emission upon *RcG/FPPS1* downregulation, genetically confirming the existence of a metabolic cross talk in rose flowers with trafficking of RcG/FPPS1-dependent isoprenoid intermediates from the cytosol to plastids. The emission of a nonterpene VOC TMB remained unaffected in flowers with decreased *RcG/FPPS1*

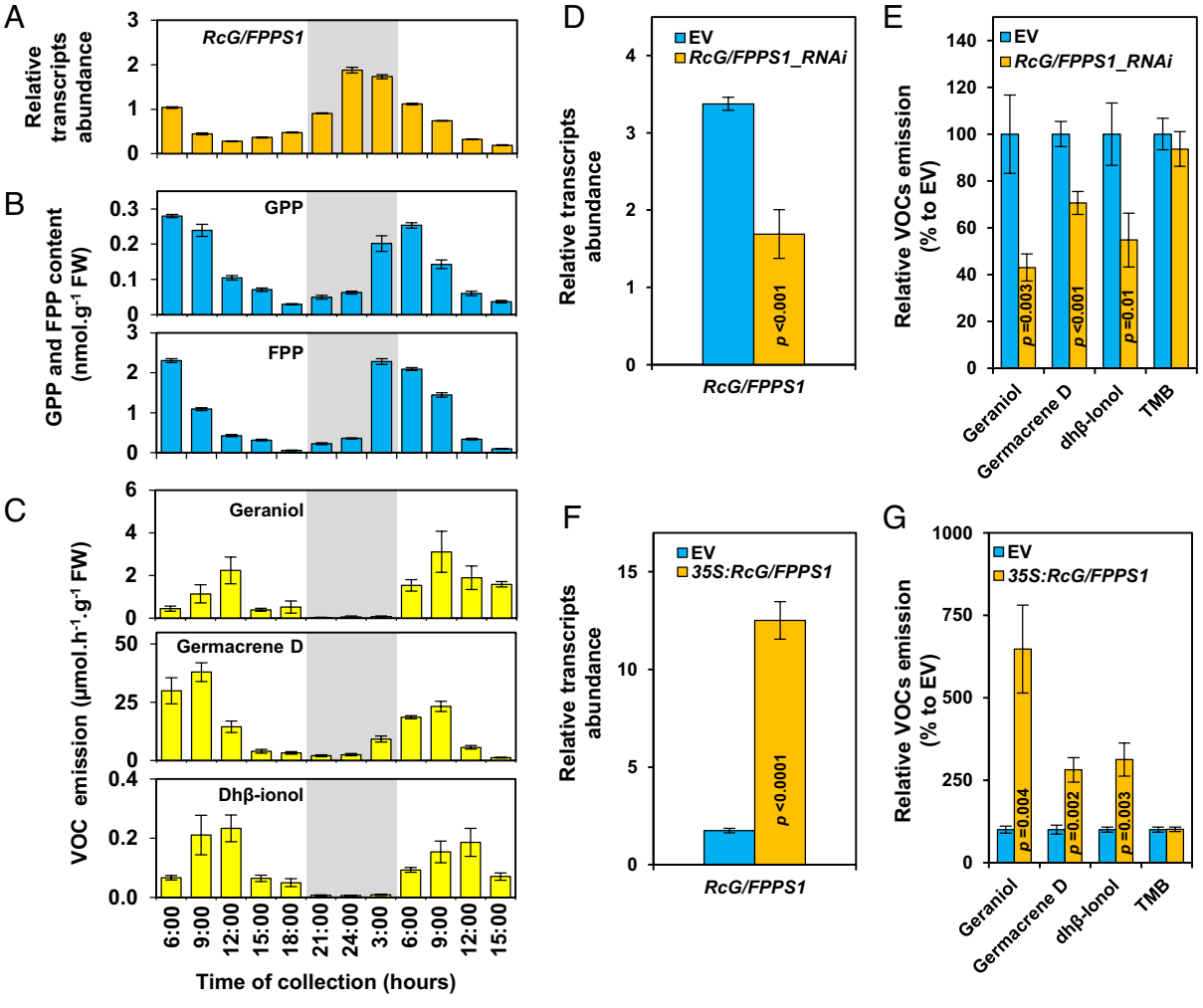

Fig. 4. Bifunctional RcG/FPPS1 plays a major role in the biosynthesis of terpenoid VOCs including geraniol in rose flowers. (*A*) RT-qPCR quantification of *RcG/FPPS1* transcript levels during a day/night cycle in RcOB petals, means ± SEM, n = 4. (*B*) LC-MS/MS quantification of GPP and FPP accumulations during a day/night cycle in RcOB petals, means ± SEM, n = 4. (*C*) GC-MS quantification of VOC emissions during a day/night cycle in RcOB petals, means ± SEM, n = 6 to 13. Night time is highlighted in gray in (*A*–*C*). (*D*) RT-qPCR quantification of *RcG/FPPS1* transcript levels in RcOB flowers agroinfiltrated with EV control or *RcG/FPPS1*_RNAi construct. (*E*) GC-MS quantification of VOCs emitted from RcOB flowers agroinfiltrated as described in (*D*). Data in (*D* and *E*) are means ± SEM, n = 12. (*F*) RT-qPCR quantification of *RcG/FPPS1* transcript levels in RcOB flowers agroinfiltrated with EV control or *35S:RcG/FPPS1* construct. (*F*) GC-MS quantification of VOCs emitted from RcOB flowers agroinfiltrated as described in (*E*). Data in *F* and *G* are means ± SEM, n = 6. *P* values in (*D*–*G*) indicate statistically significant differences compared to EV analyzed by two-tailed Student's *t* test.

transcripts (Fig. 4 *D* and *E*). These in planta results were consistent with inhibition and precursor feeding experiments (Fig. 1) as well as RcG/FPPS1 biochemical characterization (Fig. 3). Moreover, rose flowers transiently overexpressing *RcG/FPPS1* (Fig. 4*F*) emitted significantly higher levels of geraniol, germacrene D, and dhβ-ionol compared to control with unchanged TMB emission (Fig. 4*G*), further supporting RcG/FPPS1 involvement in cytosolic GPP and FPP formation.

The G/FPPS Activity Is Conserved in Rosaceae. To understand when the G/FPPS activity discovered in rose evolved from ancestral and bona fide FPPSs, we investigated the FPPS family in *Rosid* species. FPPS protein sequences were retrieved from both *Rosoideae* (*Rosa chinensis*, *Fragaria vesca,* and *Potentilla micrantha*) and *Amygdaloideae* (*Malus domestica*, *Prunus persica,* and *Prunus domestica*) subfamilies within *Rosaceae* and several *Rosid* species including previously characterized FPPSs such as *A. thaliana* and *Populus trichocarpa* FPPSs. Phylogenetic analysis and comparison of genes surrounding *RcG/FPPS1* and *RcFPPS2* (Fig. 5 *A* and *B*) enabled to place each *Rosid* FPPSs into either the FPPS1 or FPPS2 groups (highlighted on Fig. 5*A*) as orthologs according to their shared synteny with one or the other rose (G)/FPPSs. This confirmed that RcG/FPPS1 evolved from a common ancestor in *Rosids* originally exhibiting FPPS activity such as AtFPPS1 and PtFPPS1 (41, 42). To identify when the bifunctional G/FPPS activity emerged in *Rosids* within the FPPS1 group, we biochemically characterized in vitro (Fig. 5*C*) and in planta (Fig. 5*D*) several of its members including the phylogenetically distant to rose and previously characterized PtFPPS1 used as control, the uncharacterized *Medicago truncatula* MtFPPS1 belonging to the *Fabaceae* family and FPPS1s from *F. vesca* and *P. persica* from *Rosoideae* and *Amygdaloideae* subfamilies in *Rosaceae,* respectively. These analyses revealed that the G/FPPS activity is conserved in *Rosaceae* in both *Rosoideae* and *Amygdaloideae.* FvG/FPPS1 and PpG/FPPS1 produced both GPP and FPP in vitro and the coexpression of their encoding genes with *RcNUDX1-1a* in *N. benthamiana* leaves resulted, as in case with *RcG/FPPS1*, in about twofold increase in geraniol production compared to leaves expressing *RcNUDX1-1a* alone. PtFPPS1 and MtFPPS1 synthesizing mainly FPP in vitro also produced small amounts of GPP, which were fourfold and eightfold lower than that of RcG/FPPS1, respectively (Fig. 5*C*). Consistently, the coexpression of their respective genes with *RcNUDX1-1a* in *N. benthamiana* leaves resulted only in slight increase in geraniol production by ~1.2-fold compared to leaves expressing *RcNUDX1-1a* alone (Fig. 5*D*). These results suggest that GPPS activity of RcG/FPPS1 is conserved in *Rosaceae* species and probably evolved earlier than the diversification of *Rosaceae* species in *Rosid* species.

At Least Two Amino Acid Residues Are Responsible for the Emergence of the GPPS Activity in Rosaceae G/FPPS. To investigate how the G/FPPS activity appeared during evolution, *Rosaceae* G/FPPS1 protein sequences were searched for conserved amino acid residues which are different from the bona fide FPPSs from *Rosids* known to produce FPP. The sequence alignment showed that a short QLLQ motif at positions 59-62 (QLLQ59-62), the phenylalanine residue 88 (F88), and the valine residue 123 (V123) are strictly conserved in the *Rosaceae* G/FPPSs but not in the FPPSs (Fig. 6*A*). In-depth analysis of all *Rosaceae* FPPS1 sequences retrieved from available *Rosaceae* genomes in the Genome Database for *Rosaceae* (GDR) confirmed that these motifs are strictly conserved in all *Rosaceae* FPPS1s when compared to FPPS1s from *Rosids* (*SI Appendix*, Fig. S5). To test whether these conserved residues contribute to gaining the GPPS activity by the bona fide FPPSs, a computational strategy combining homology-based modeling with molecular dynamics (MD) simulations was used. Before generating the model, the homodimeric state of active RcG/FPPS1 was verified by copurification of 6-His-tagged RcG/FPPS1 with untagged RcG/FPPS1 (*SI Appendix*, Fig. S3*B*) and by size-exclusion chromatography followed by activity analysis (*SI Appendix*, Fig. S3*C*). Indeed, active RcG/FPPS1 formed a homodimer of 78 kDa. Thus, homodimeric model was generated, and binding free energies for GPP in the presence of IPP and Mg^{2+} ions, which mimic the substrate-binding step for FPPS activity, were calculated for the wild-type (WT) RcG/FPPS1 and its in silico mutant versions for the identified conserved residues, which harbored amino acids from bona fide orthologous FPPSs. Mutating independently either F88 to Y88 and V123 to I123 but not QLLQ59-62 to KLLK59-62 resulted in significantly lower GPP-binding free energies (Fig. 6*B*) corresponding to a stronger GPP–enzyme interaction. This suggested that Y88 and I123 in ancestral orthologs favor FPP production and their substitutions to F88 and V123 during *Rosaceae* evolution could be responsible for gaining GPPS activity.

To validate the model prediction and examine the contribution of each conserved residue on the G/FPPS activity, several RcG/FPPS1 mutants containing single or multiple mutations were generated by site-directed mutagenesis, and the corresponding recombinant proteins were biochemically characterized. Consistent with the model prediction, both F88Y and V123I substitutions independently reduced GPP formation by 55% compared to WT RcG/FPPS1 with a simultaneous increase in FPP formation (Fig. 6*C*). A synergistic effect was detected in the double mutant (F88Y/V123I) with GPP production further reduced by an additional 45%. Kinetic analysis of both single and double mutants revealed that both F88Y and V123I substitutions significantly increase (3.6 to 5.9-fold) the affinity of proteins for IPP in the presence of GPP as cosubstrate (Table 1), thus making the mutated RcG/FPPS1 biochemically very similar to the phylogenetically distant RcFPPS2 although the latter produces almost exclusively FPP (Fig. 6*C*). Moreover, *N. benthamiana* leaves coexpressing *RcNUDX1-1a* with each single-mutant *RcG/FPPS1-F88Y* or *RcG/FPPS1-V123I* produced significantly less geraniol glycosides than leaves coexpressing *RcNUDX1-1a* with the native WT *RcG/FPPS1* (Fig. 6*D*). Coexpression of *RcNUDX1-1a* with the double-mutant *RcG/FPPS-F88Y-V123I* further decreased geraniol production. When the opposite mutations, Y88F and I123V, were introduced into RcFPPS2, the recombinant mutant enzyme started to release GPP as a product (Fig. 6*C*). Substitutions of Q to K in the QLLQ59-62 motif had no effect on the G/FPPS activity of RcG/FPPS1 neither alone nor in combination with F88Y/V123I (Fig. 6*C*).

Further in silico comparative structural analyses of RcG/FPPS1 WT and mutant models after 1,500 ps of MD simulations revealed that in contrast to RcG/FPPS1 WT, mutants harboring F88Y substitution exhibit a quick formation of a hydrogen bond between the introduced tyrosine in each subunit (Y88–Y88′) of the homodimer (Fig. 6*E* and *SI Appendix*, Fig. S6*A*). Models also showed that the ancestral isoleucine from each subunit (I123–I123′) are positioned in proximity to the Y88–Y88′ pair (Fig. 6*E*). WT F88 or ancestral Y88 is located 5 amino acids before the conserved first aspartate motif (FARM) known to be crucial for allylic substrate binding (43). They are also located one amino acid before P89. This bulky aromatic residue is known to define the floor of the pocket that forms at the interface of both subunits (Fig. 6*E*) and in which the hydrocarbon chain of the allylic substrates binds before product elongation (44–46). Previous studies on avian, microbial, and insect FPPSs showed that mutations of

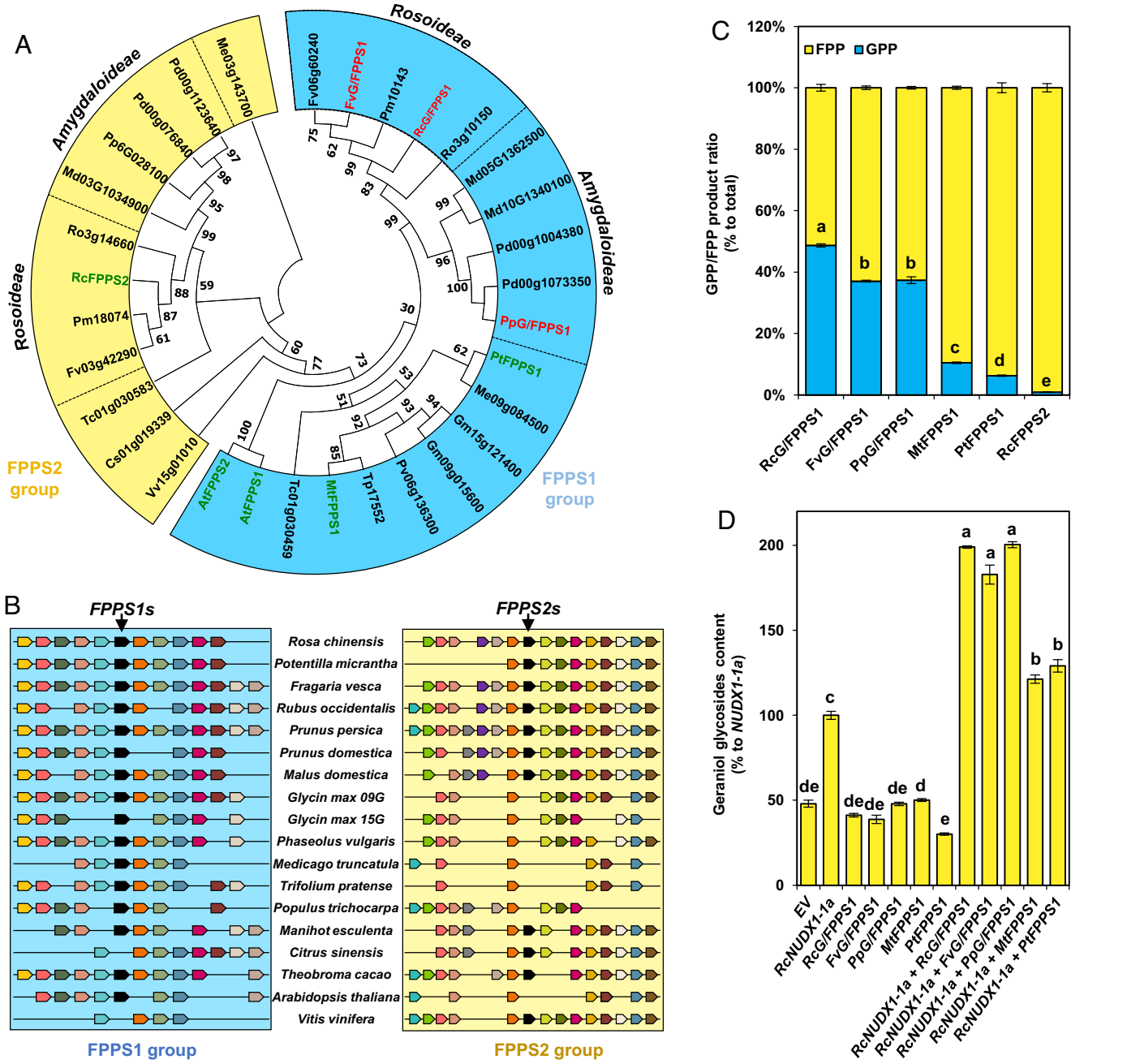

Fig. 5. The bifunctional G/FPPS activity is conserved in *Rosaceae*. (*A*) Maximum likelihood tree of *Rosid* FPPSs from RcOB (Rc), *Arabidopsis thaliana* (At), *Citrus sinensis* (Cs), *Fragaria vesca* (Fv), *Glycine max* (Gm), *Malus domestica* (Md), *Manihot esculenta* (Me), *Medicago truncatula* (Mt), *Prunus dulcis* (Pd), *Phaseolus vulgaris* (Pv), *Populus trichocarpa* (Pt), *Potentilla micrantha* (Pm), *Prunus persica* (Pp), *Rubus occidentalis* (Ro), *Theobroma cacao* (Tc), *Trifolium pratense* (Tp), and *Vitis vinifera* (Vv). Numbers correspond to bootstrap values. FPPS1 (blue) and FPPS2 (orange) groups are highlighted and were defined according to phylogeny and synteny analysis (See *B*). Characterized FPPSs are depicted in green and characterized G/FPPS1s are depicted in red. (*B*) Microsynteny of *Rosids* genes encoding for FPPSs from FPPS1 and FPPS2 groups as used in *A*. (*C*) LC-MS/MS quantification of the GPP/FPP product ratio formed by 250 ng of the indicated FPPSs incubated for 20 min with 10 μM DMAPP and IPP. Data are means ± SEM, n = 3. (*D*) LC-MS/MS quantification of geraniol glycosides accumulating in *Nicotiana benthamiana* leaves transiently expressing the indicated *FPPSs* alone or in coexpression with *RcNUDX1-1a*. Data are relative quantification to *NUDX1-1a* set at 100 %, mean ± SEM, n = 4. Letters in *C* and *D* indicate statistically significant differences analyzed by ANOVA and Tukey post-hoc test.

residues involved in the formation of this binding pocket, and especially those located −1, −4, and −5 before FARM, can alter product chain length (*SI Appendix*, Fig. S7) (44–50). In RcG/FPPS1 WT, the absence of hydrogen bond formation observed between the ancestral Y88–Y88′ pair and the presence of V123 instead of ancestral I123 modify the protein–protein interaction between both subunits. This likely alters the pocket conformation (Fig. 6*E*) and reduces GPP-enzyme binding (Fig. 6*B*), leading to GPP release. In addition, based on the RMSF profiles of the MD simulations, all mutants with reduced GPPS activity and especially those harboring the F88Y mutation displayed apparent movement of four basic amino acid residues (KRKK) located at the C terminus in contrast to WT RcG/FPPS1 and K59Q/K62Q mutants (Fig. 6*F*). The superimposed structures of WT, F88Y, and F88Y/V123I double mutant revealed a trend of C terminus closure toward the active site within MD simulation (*SI Appendix*, Fig. S6*B*). This movement is known to be required for FPPS activity as the KRKK motif interacts with the negatively charged diphosphate group of IPP during catalysis (51). The absence of such movement in WT RcG/FPPS1 within MD simulations

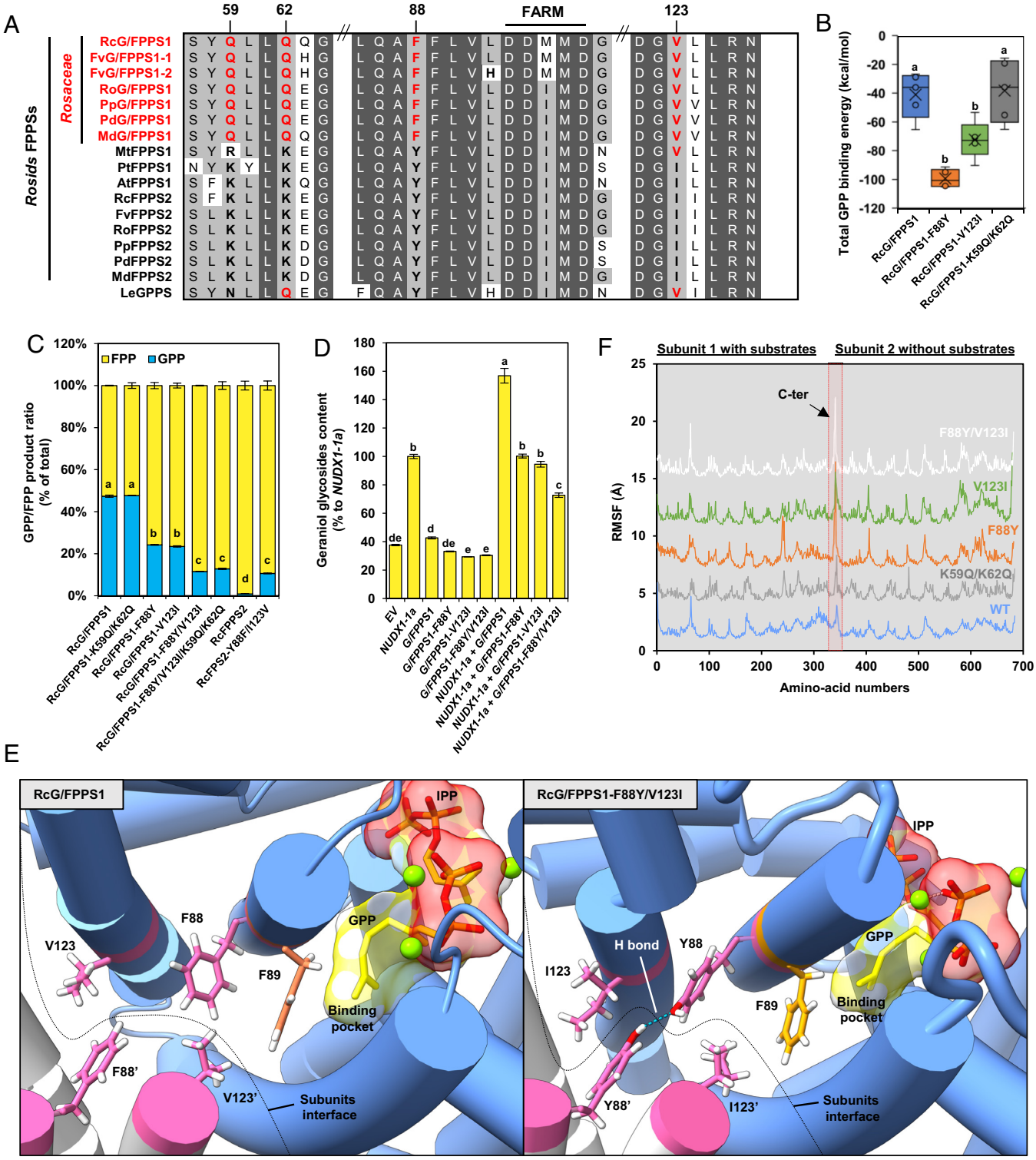

Fig. 6. Two amino acids are critical for the GPPS activity of RcG/FPPS1. (*A*) Protein sequence alignment of *Rosid* FPPS1s and FPPS2s including *Rosaceae* G/FPPS1s (red). Only relevant sequence parts are shown to highlight residues conserved in *Rosaceae* G/FPPS1s (red) compared to bona fide FPPS1s and FPPS2s. (*B*) Binding free energies of GPP for RcG/FPPS1 and its mutated versions F88Y, V123I, and K59Q/K62Q after 1,500 ps of MD simulations with GPP, IPP, and Mg^{2+} placed in the active site. Data are means ± SEM of the five last recorded conformations. (*C*) LC-MS/MS quantification of the GPP/FPP product ratio formed by the indicated recombinant proteins incubated for 20 min with 10 µM DMAPP and IPP. Data are means ± SEM, n = 3. (*D*) LC-MS/MS quantification of geraniol glycosides accumulated in *Nicotiana benthamiana* leaves transiently expressing the indicated genes alone or in coexpression with *RcNUDX1-1a*. Data are relative quantification to *RcNUDX1-1a* set at 100 %, mean ± SEM, n = 4. Letters in *B–D* indicate statistically significant differences between samples analyzed by ANOVA and Tukey post-hoc test. (*E*) Models of WT RcG/FPPS1 homodimer and its mutated version RcG/FPPS1-F88Y/V123I at 1,500 ps of MD simulation as described in (*B*). The model focuses on the interaction of both protein subunits around the amino acid pairs Y88–Y′88 and V123–V123′ (pink), the binding pockets for GPP with the hydrocarbon chain (yellow) and phosphate groups (red), and the aromatic residue F89 forming the extremity of the pocket (orange). The Mg_2^+ ions (green balls), the hydrogen bond between the Y88–Y88′ amino acid pair (blue dashed line), and the subunits' interface (black dashed line) are shown. (*F*) Root mean square fluctuations (RMSF) of each amino acid of RcG/FPPS1 homodimer and its mutated versions during the 1,500 ps of MD simulation as described in (*C*). The C terminus of subunit 1 displaying improved movements in mutants compared to WT RcG/FPPS1 is highlighted.

suggests that both amino acids, F88 and V123, located at the subunits' interface, likely affect the flexibility of distal regions of the enzyme, making further GPP conversion to FPP less favorable and fast resulting in GPP release. Taken together, these results suggest that F88 and V123 which evolved from ancestral Y88 and I123, respectively, are crucial for bifunctional G/FPPS activity.

Discussion

It is generally accepted that in most plants, monoterpenes are produced in plastids by monoterpene synthases using GPP derived from the MEP pathway (6). However, to date, several reports showed that there are monoterpene synthases naturally targeted to the cytosol (14, 15, 52) as well as bifunctional cytosolic mono-/sesquiterpene synthases capable of producing monoterpenes (14, 18). Also, targeting monoterpene synthases to the cytoplasm by metabolic engineering resulted in monoterpene formation, suggesting that the GPP pool exists in this cellular compartment (14, 15, 17–20, 53). In addition, the involvement of cytosolic NUDX enzymes in geraniol production was recently discovered in roses (3) and pelargonium (54), and biosynthesis of shikonin from cytosolic GPP was reported in *L. erythrorhizon* (12, 13). Although cytosolic GPP could originate via cross talk from the MEP pathway, feeding experiments with labeled precursors in *F. vesca*, *Rubus idaeus*, *R.* x *hybrida* (55–57), and in *L. erythrorhizon* (58) suggested that the MVA pathway is the major contributor to the biosynthesis of monoterpenes and GPP-derived compounds in these plant species. Recently, *LeGPPS* encoding a cytosolic GPPS involved in shikonin biosynthesis has been isolated and characterized from *L. erythrorhizon* (32, 33), but it still remained unknown how cytosolic GPP production is achieved in plants and especially in roses for RcNUDX1-1a-dependent geraniol biosynthesis and in other *Rosaceae* for MVA-dependent monoterpene formation. Here, we provide biochemical (Fig. 3, *SI Appendix*, Fig. S2, and Table 1) and genetic evidences (Figs. 3*D* and 4 *D*–*G*) that a cytosolic bifunctional RcG/FPPS1 (Figs. 2*C* and 3*A*) is involved in GPP biosynthesis in rose petals. This homodimeric enzyme, belonging to FPPS family (Fig. 2*A*), keeps its ability to synthesize FPP but produces GPP 15-fold more efficiently (k_{cat}/K_m ratio) than FPP in vitro (Table 1) and is the only one out of the five identified rose IDS candidates able to provide cytosolic GPP substrate for RcNUDX1-1a in planta (Fig. 3*D*).

The biochemical characterization of orthologous FPPSs from several *Rosid* species guided by phylogenetic analysis showed that the bifunctional G/FPPS activity emerged during evolution of *Rosids* from the bona fide FPPSs and was conserved in *Rosaceae* including RcOB, *F. vesca,* and *P. persica* (Fig. 5). Moreover, these results uncovered a so far unknown characteristic property of the FPPS1 clade. Members of the FPPS1 group (MtFPPS1 and PtFPPS1), but not FPPS2, exhibit dual activity despite producing GPP at lower levels and less efficiently than *Rosaceae* G/FPPs (Fig. 5 *C* and *D*). This residual GPPS activity of cytosolic FPPS1s could contribute to the cytosolic GPP pool used for the synthesis of geranylated plant secondary metabolites such as cannabinoids and flavonoids for example ref. 59 or for yet unknown mechanism of RNA or peptide geranylation reported in bacteria (60, 61). At least two amino acids F88 and V123, which are highly conserved in *Rosaceae,* are responsible for efficient GPP production in addition to FPP by G/FPPSs (Fig. 6 and *SI Appendix*, Fig. S5). They modulate the affinity of enzymes toward GPP substrate and the product selectivity in favor of GPP production in addition to keeping FPP production (Table 1). The reasons why these mutations were selected during evolution for high cytosolic production of monoterpenes in specialized plant organs (14) are currently unknown. It is possible that G/FPPS were selected during evolution because of the deficient capacity of plastidic heterodimeric GPPS to produce GPP efficiently as observed in roses (Fig. 3, *SI Appendix*, Fig. S2, and Table 1). Moreover, these results also provide an answer to a long-standing question about the cytosolic and MVA-dependent monoterpene production in strawberries, raspberries, and roses (14, 55–57) (Fig. 5*C*). The noncanonical biosynthetic pathway for geraniol production in roses requires both GPP availability and NUDX1-1a enzyme in the cytosol. While the NUDX1-1a specialization appeared during the diversification of *Rosa* genus (5), our results show that the ability to synthesize the cytosolic GPP preceded NUDX1-1a acquisition in several *Rosaceae* genus, indicating that two evolutionary events enabled high geraniol production in rose flowers.

FPPSs' structure and mechanism have been extensively studied due to their involvement in processes essential for cell survival (62). Naturally, GPP is an intermediate product of typical FPPSs. Numerous studies on avian, bacterial, and yeast FPPSs showed that FPPSs can release GPP and that the nature of residues involved in the formation of the binding pocket for the allylic substrates, and especially those positioned −1, −4, and −5 before FARM, is crucial for product specificity (*SI Appendix*, Fig. S7) (44–50). The first FPPS capable to generate both GPP and FPP has been identified in aphids for which the motifs −1 and −4 before FARM were shown to be essential for its bifunctionality (48, 49). Our MD simulation and site-directed mutagenesis of RcG/FPPS1 revealed that the F88–F88′ pair, located at position FARM -5 (Fig. 6*A*), and the V123–V123′ pair positioned in its proximity (Fig. 6*E*), are both involved in protein–protein interaction and are crucial for GPPS activity (Fig. 6 *C* and *D*). Interestingly, EuFPPS1 from hardy rubber tree (*Eucommia ulmoides*), which possesses Y88 and I123, produces mostly FPP in vitro while EuFPPS2, which contains F88 and V123, produces GPP in addition to FPP similarly to *Rosaceae* G/FPPS1s (63). In contrast, in *L. erythrorhizon,* LeGPPS produces exclusively GPP and possess H100 residue at position FARM -1 (Fig. 6*A* and *SI Appendix*, Fig. S7) which was shown to contribute to product specificity (32). The three *Rosaceae* G/FPPS1 characterized in this study, RcG/FPPS1, FvG/FPPS1-1, and PpG/FPPS1 (Fig. 5 *C* and *D*), contain L100 instead of H100. Interestingly, FvG/FPPS1-2 contains H100 in addition to F88 and V123 (Fig. 6*A*), but its activity was extremely low compared to the other characterized *Rosaceae* G/FPPS1s (*SI Appendix*, Fig. S8). Taken together, these results suggest that the emergence of cytosolic GPPS activity occurred independently from bona fide FPPSs in phylogenetically distant species including plants (*Rosaceae, Boraginaceae,* and *Eucommiaceae)* and insects via convergent evolutionary mechanisms.

The discovery of bifunctional G/FPPSs suggests that plants have two types of homodimeric GPPSs in addition to heterodimeric ones. All previously characterized homodimeric GPPSs are evolutionarily related to GGPPSs forming a GGPPS-like group (6), two members of which, from *Quercus robur* (22) and *Phalaenopsis bellina* (24), were shown to produce GPP and FPP in vitro. In contrast, recently isolated LeGPPS (32) and *Rosaceae* G/FFPSs identified in this study are evolutionarily related to FPPSs. Within this FPPSs-like group, there are two types of enzymes: bifunctional enzymes like RcG/FFPS1, FvG/FPPS1, and PpG/FPPS1 (Fig. 5*C*) and monofunctional enzymes with strict product specificity like LeGPPS. Moreover, members of the FPPSs-like group are localized in the cytosol (Fig. 2*C* and ref. 32) in contrast to the heterodimeric GPPSs, which are always found in the plastids and homodimeric GPPSs most of which are either localized in plastids or mitochondria (22–25). Overall,

our discovery of cytosolic GPP formation in *Rosaceae* along with *L. erythrorhizon* and other reports of plant FPPSs producing GPP in vitro (63, 64) (*SI Appendix*, Table S2) suggest that this phenomenon, although likely species specific, could be widespread in plant kingdom. Cytosolic plant FPPSs can also produce small or trace amount of GPP in addition to FPP when evaluated in vitro which is evident from presented radio TLC runs, radio GC, GC-MS, and LC-MS profiles of their products (summarized in *SI Appendix*, Table S2). Unfortunately, in these studies, the GPP/FPP ratios were rarely quantified and the ability of these FPPSs to produce cytosolic GPP in vivo was not tested, as well as no experiments with pathway-specific inhibitors or precursors to support cytosolic GPP formation were performed. Thus, further thorough reevaluation of FPPSs' functions in vitro and in vivo will uncover how widely FPPSs are used for cytosolic GPP and monoterpene production in plants.

Materials and Methods

Details about plant material, plant growth conditions, and chemicals are described in *SI Appendix, Materials and Methods*. Chemical synthesis, inhibitory and stable isotope-labeling experiments, VOC collection, GC-MS analysis, subcellular GPPS and FPPS activities, phylogeny and synteny analyses, sampling procedure for gene expression analysis and metabolite profiling, gene expression analyses, generation of vector constructs, in vitro assays, size-exclusion chromatography, in planta biochemical characterization, LC-MS/MS analysis, transitory down- and up-regulation homology modeling, and MD simulations were performed according to protocols described in *SI Appendix, Materials and Methods*.

Data, Materials, and Software Availability. RNA-seq data have been deposited in the National Center for Biotechnology Information (NCBI) Sequence Read Archive (SRA) under the BioProject accessions: PRJNA911487 (65) and PRJNA911454 (66). All study data are included in the article and/or *SI Appendix*.

ACKNOWLEDGMENTS. This work was supported by Agence Nationale de la Recherche (grant number ANR-16-CE20-0024-01 to S.B.). This work was supported by the grant from the National Science Foundation IOS-1655438 and by the USDA National Institute of Food and Agriculture Hatch Project number 177845 to N.D. We thank Andréa Hemmerlin for sharing the pRSF-DUET vector.

Author affiliations: [a]Université Jean Monnet Saint-Etienne, Centre National de la Recherche Scientifique, Laboratoire de Biotechnologies Végétales appliquées aux Plantes Aromatiques et Médicinales, Unité Mixte de Recherche 5079, Saint-Etienne F-42023, France; [b]Department of Biochemistry, Purdue University, West Lafayette, IN 47907-2063; [c]Institut de Biologie Moléculaire des Plantes du Centre National de la Recherche Scientifique, Unité Propre de Recherche 2357, Université de Strasbourg, Strasbourg 67084, France; [d]Department of Vegetable Crops, Newe Ya'ar Research Center, Agricultural Research organization, The Volcani Center, Ramat Yishay 30095, Israel; [e]Department of Vegetable Crops, The Robert Smith Faculty of Agriculture, Food and Environment, The Hebrew University of Jerusalem, Rehovot 76100001, Israel; [f]Université de Lyon, Centre National de la Recherche Scientifique, Université Claude Bernard Lyon 1, Institut des Sciences Analytiques, UMR 5280, Villeurbanne F-69100, France; [g]Université d'Angers, Institut Agro, Institut National de Recherche pour l'Agriculture, l'Alimentation et l'Environnement, Institut de Recherche en Horticulture et Semences, Structure Fédérative de Recherche Qualité et Santé du Végétal, Angers 49000, France; [h]Nalecz Institute of Biocybernetics and Biomedical Engineering, Polish Academy of Sciences, Warsaw 02-109 Poland; [i]Institute of Biochemistry and Biophysics, Polish Academy of Sciences, Warsaw 02-106 Poland; [j]Université de Strasbourg, Institut National de Recherche pour l'Agriculture, l'Alimentation et l'Environnement, Unité Mixte de Recherche 1131 Santé de la Vigne et Qualité du Vin, F-68000 Colmar, France; [k]Institut de Chimie de Strasbourg, Université de Strasbourg/Centre National de la Recherche Scientifique, Unité Mixte de Recherche 7177, Institut Le Bel, Strasbourg 67081, France; [l]Purdue Center for Plant Biology, Purdue University, West Lafayette, IN 47907; and [m]Department of Horticulture and Landscape Architecture, Purdue University, West Lafayette, IN 47907-2010

1. Z. Xiao, J. Li, Y. Niu, Q. Liu, J. Liu, Verification of key odorants in rose oil by gas chromatography–olfactometry/aroma extract dilution analysis, odour activity value and aroma recombination. *Nat. Prod. Res.* **31**, 2294–2302 (2017).
2. Y. Iijima, D. R. Gang, E. Fridman, E. Lewinsohn, E. Pichersky, Characterization of geraniol synthase from the peltate glands of sweet basil. *Plant Physiol.* **134**, 370–379 (2004).
3. J. L. Magnard *et al.*, Biosynthesis of monoterpene scent compounds in roses. *Science (1979)* **349**, 81–83 (2015).
4. J. R. Srouji, A. Xu, A. Park, J. F. Kirsch, S. E. Brenner, The evolution of function within the Nudix homology clan. *Proteins* **85**, 775–811 (2017).
5. C. Conart *et al.*, Duplication and specialization of *NUDX1* in *Rosaceae* led to geraniol production in rose petals. *Mol. Biol. Evol.* **39**, msac002 (2022).
6. D. Tholl, Biosynthesis and biological functions of terpenoids in plants. *Adv. Biochem. Eng. Biotechnol.* **148**, 63–106 (2015).
7. A. Hemmerlin, J. L. Harwood, T. J. Bach, A raison d'être for two distinct pathways in the early steps of plant isoprenoid biosynthesis? *Prog. Lipid Res.* **51**, 95–148 (2012).
8. E. Vranová, D. Coman, W. Gruissem, Structure and dynamics of the isoprenoid pathway network. *Mol. Plant* **5**, 318–333 (2012).
9. M. Á. Ruiz-Sola *et al.*, A single *Arabidopsis* gene encodes two differentially targeted geranylgeranyl diphosphate synthase isoforms. *Plant Physiol.* **172**, 1393–1402 (2016).
10. K. Okada, T. Saito, T. Nakagawa, M. Kawamukai, Y. Kamiya, Five geranylgeranyl diphosphate synthases expressed in different organs are localized into three subcellular compartments in *Arabidopsis*. *Plant Physiol.* **122**, 1045–1056 (2000).
11. M. Herde *et al.*, Identification and regulation of TPS04/GES, an *Arabidopsis* geranyllinalool synthase catalyzing the first step in the formation of the insect-induced volatile C16-homoterpene TMTT. *Plant Cell* **20**, 1152–1168 (2008).
12. S. Sommer, K. Severin, B. Camara, L. Heide, Intracellular localization of geranylpyrophosphate synthase from cell cultures of *Lithospermum erythrorhizon*. *Phytochemistry* **38**, 623–627 (1995).
13. L. Heide, U. Berger, Partial purification and properties of geranyl pyrophosphate synthase from *Lithospermum erythrorhizon* cell cultures. *Arch. Biochem. Biophys.* **273**, 331–338 (1989).
14. A. Aharoni *et al.*, Gain and loss of fruit flavor compounds produced by wild and cultivated strawberry species. *Plant Cell* **16**, 3110–3131 (2004).
15. L. Dong *et al.*, Characterization of two geraniol synthases from *Valeriana officinalis* and *Lippia dulcis*: Similar activity but difference in subcellular localization. *Metab. Eng.* **20**, 198–211 (2013).
16. V. Falara *et al.*, The tomato terpene synthase gene family. *Plant Physiol.* **157**, 770–789 (2011).
17. L. Dong, E. Jongedijk, H. Bouwmeester, A. Van Der Krol, Monoterpene biosynthesis potential of plant subcellular compartments. *New Phytol.* **209**, 679–690 (2016).
18. R. Davidovich-Rikanati *et al.*, Overexpression of the lemon basil α-zingiberene synthase gene increases both mono- and sesquiterpene contents in tomato fruit. *Plant J.* **56**, 228–238 (2008).
19. S. Wu *et al.*, Redirection of cytosolic or plastidic isoprenoid precursors elevates terpene production in plants. *Nat. Biotechnol.* **24**, 1441–1447 (2006).
20. K. Ohara, Limonene production in tobacco with perilla limonene synthase cDNA. *J. Exp. Bot.* **54**, 2635–2642 (2003).
21. T. H. Chang *et al.*, Structure of a heterotetrameric geranyl pyrophosphate synthase from mint (*Mentha piperita*) reveals intersubunit regulation. *Plant Cell* **22**, 454–467 (2010).
22. A. Schmidt, J. Gershenzon, Cloning and characterization of two different types of geranyl diphosphate synthases from Norway spruce (*Picea abies*). *Phytochemistry* **69**, 49–57 (2008).
23. A. Rai, S. S. Smita, A. K. Singh, K. Shanker, D. A. Nagegowda, Heteromeric and homomeric geranyl diphosphate synthases from *Catharanthus roseus* and their role in monoterpene indole alkaloid biosynthesis. *Mol. Plant* **6**, 1531–1549 (2013).
24. Y. Y. Hsiao *et al.*, A novel homodimeric geranyl diphosphate synthase from the orchid *Phalaenopsis bellina* lacking a DD(X)2–4D motif. *Plant J.* **55**, 719–733 (2008).
25. C. Burke, R. Croteau, Geranyl diphosphate synthase from *Abies grandis*: cDNA isolation, functional expression, and characterization. *Arch. Biochem. Biophys.* **405**, 130–136 (2002).
26. A. Schmidt *et al.*, A bifunctional geranyl and geranylgeranyl diphosphate synthase is involved in terpene oleoresin formation in *Picea abies*. *Plant Physiol.* **152**, 639–655 (2010).
27. G. Hivert *et al.*, Prenyltransferases catalyzing geranyldiphosphate formation in tomato fruit. *Plant Sci.* **296**, 110504 (2020).
28. C. Burke, R. Croteau, Interaction with the small subunit of geranyl diphosphate synthase modifies the chain length specificity of geranylgeranyl diphosphate synthase to produce geranyl diphosphate. *J. Biol. Chem.* **277**, 3141–3149 (2002).
29. D. Tholl *et al.*, Formation of monoterpenes in *Antirrhinum majus* and *Clarkia breweri* flowers involves heterodimeric geranyl diphosphate synthases. *Plant Cell* **16**, 977–992 (2004).
30. I. Orlova *et al.*, The small subunit of snapdragon geranyl diphosphate synthase modifies the chain length specificity of tobacco geranylgeranyl diphosphate synthase in planta. *Plant Cell* **21**, 4002–4017 (2009).
31. G. Wang, R. A. Dixon, Heterodimeric geranyl(geranyl)diphosphate synthase from hop (*Humulus lupulus*) and the evolution of monoterpene biosynthesis. *Proc. Natl. Acad. Sci. U.S.A.* **106**, 9914–9919 (2009).
32. H. Ueoka *et al.*, A cytosol-localized geranyl diphosphate synthase from *Lithospermum erythrorhizon* and its molecular evolution. *Plant Physiol.* **182**, 1933–1945 (2020).
33. T. Suttiyut *et al.*, Integrative analysis of the shikonin metabolic network identifies new gene connections and reveals evolutionary insight into shikonin biosynthesis. *Hortic. Res.* **9**, uhab087 (2022).
34. J. A. Bick, B. M. Lange, Metabolic cross talk between cytosolic and plastidial pathways of isoprenoid biosynthesis: Unidirectional transport of intermediates across the chloroplast envelope membrane. *Arch. Biochem. Biophys.* **415**, 146–154 (2003).
35. L. Hibrand-Saint Oyant *et al.*, A high-quality genome sequence of *Rosa chinensis* to elucidate ornamental traits. *Nat. Plants* **4**, 473–484 (2018).
36. O. Raymond *et al.*, The *Rosa* genome provides new insights into the domestication of modern roses. *Nat. Genet.* **50**, 772–777 (2018).
37. I. Guterman *et al.*, Rose scent: Genomics approach to discovering novel floral fragrance-related genes. *Plant Cell* **14**, 2325–2338 (2002).
38. F. C. Huang, P. Molnár, W. Schwab, Cloning and functional characterization of carotenoid cleavage dioxygenase 4 genes. *J. Exp. Bot.* **60**, 3011–3022 (2009).
39. G. Scalliet *et al.*, Biosynthesis of the major scent components 3,5-dimethoxytoluene and 1,3,5-trimethoxybenzene by novel rose O-methyltransferases. *FEBS Lett.* **523**, 113–118 (2002).
40. S. Takahashi *et al.*, Kinetic and molecular analysis of 5-epiaristolochene 1,3-dihydroxylase, a Cytochrome P450 enzyme catalyzing successive hydroxylations of sesquiterpenes. *J. Biol. Chem.* **280**, 3686–3696 (2005).
41. N. Cunillera *et al.*, *Arabidopsis thaliana* Contains two differentially expressed farnesyl-diphosphate synthase genes. *J. Biol. Chem.* **271**, 7774–7780 (1996).

42. N. D. Lackus *et al.*, Identification and characterization of trans-isopentenyl diphosphate synthases involved in herbivory-induced volatile terpene formation in *Populus trichocarpa*. *Molecules* **24** (2019).
43. L. C. Tarshis, J. C. Sacchettini, M. Yan, C. D. Poulter, Crystal Structure of Recombinant Farnesyl Diphosphate Synthase at 2.6-Å Resolution. *Biochemistry* **33**, 10871–10877 (1994).
44. S. M. S. Fernandez, B. A. Kellogg, C. D. Poulter, Farnesyl diphosphate synthase. Altering the catalytic site to select for geranyl diphosphate activity. *Biochemistry* **39**, 15316–15321 (2000).
45. L. C. Tarshis, P. J. Proteau, B. A. Kellogg, J. C. Sacchettini, C. D. Poulter, Regulation of product chain length by isoprenyl diphosphate synthases. *Proc. Natl. Acad. Sci. U.S.A.* **93**, 15018–15023 (1996).
46. S. Ohnuma *et al.*, A role of the amino acid residue located on the fifth position before the first aspartate-rich motif of farnesyl diphosphate synthase on determination of the final product. *J. Biol. Chem.* **271**, 30748–30754 (1996).
47. K. Narita, S.-I. Ohnuma, T. Nishino, Protein design of geranyl diphosphate synthase. Structural features that define the product specificities of prenyltransferases. *J. Biochem.* **126**, 566–571 (1999).
48. S. Vandermoten *et al.*, Characterization of a novel aphid prenyltransferase displaying dual geranyl/farnesyl diphosphate synthase activity. *FEBS Lett.* **582**, 1928–1934 (2008).
49. S. Vandermoten *et al.*, Structural features conferring dual geranyl/farnesyl diphosphate synthase activity to an aphid prenyltransferase. *Insect Biochem. Mol. Biol.* **39**, 707–716 (2009).
50. C. Ignea, M. Pontini, M. E. Maffei, A. M. Makris, S. C. Kampranis, Engineering monoterpene production in yeast using a synthetic dominant negative geranyl diphosphate synthase. *ACS Synth. Biol.* **3**, 298–306 (2014).
51. L. Song, C. D. Poulter, Yeast farnesyl-diphosphate synthase: Site-directed mutagenesis of residues in highly conserved prenyltransferase domains I and II. *Proc. Natl. Acad. Sci. U.S.A.* **91**, 3044–3048 (1994).
52. F. Zhou, E. Pichersky, The complete functional characterisation of the terpene synthase family in tomato. *New Phytol.* **226**, 1341–1360 (2020).
53. M. Gutensohn *et al.*, Cytosolic monoterpene biosynthesis is supported by plastid-generated geranyl diphosphate substrate in transgenic tomato fruits. *Plant J.* **75**, 351–363 (2013).
54. M. E. Bergman, M. Bhardwaj, M. A. Phillips, Cytosolic geraniol and citronellol biosynthesis require a Nudix hydrolase in rose-scented geranium (*Pelargonium graveolens*). *Plant J.* **107**, 493–510 (2021).
55. D. Hampel, A. Mosandl, M. Wüst, Biosynthesis of mono- and sesquiterpenes in strawberry fruits and foliage: 2H labeling studies. *J. Agric. Food. Chem.* **54**, 1473–1478 (2006).
56. D. Hampel, A. Swatski, A. Mosandl, M. Wüst, Biosynthesis of monoterpenes and norisoprenoids in raspberry fruits (*Rubus idaeus* L.): The role of cytosolic mevalonate and plastidial methylerythritol phosphate pathway. *J. Agric. Food. Chem.* **55**, 9296–9304 (2007).
57. M. J. O. Francis, M. O'Connell, The incorporation of mevalonic acid into rose petal monoterpenes. *Phytochemistry* **8**, 1705–1708 (1969).
58. H. Inouye, S. Ueda, K. Inoue, H. Matsumura, Biosynthesis of shikonin in callus cultures of *Lithospermum erythrorhizon*. *Phytochemistry* **18**, 1301–1308 (1979).
59. W. J. C. de Bruijn, M. Levisson, J. Beekwilder, W. J. H. van Berkel, J. P. Vincken, Plant aromatic prenyltransferases: Tools for microbial cell factories. *Trends in Biotechnol.* **38**, 917–934 (2020).
60. R. Wang *et al.*, Synthesis, base pairing and structure studies of geranylated RNA. *Nucleic Acids Res.* **44**, 6036–6045 (2016).
61. M. Morita *et al.*, Post-translational tyrosine geranylation in cyanobactin biosynthesis. *J. Am. Chem. Soc.* **140**, 6044–6048 (2018).
62. S. Vandermoten, É. Haubruge, M. Cusson, New insights into short-chain prenyltransferases: Structural features, evolutionary history and potential for selective inhibition. *Cell. Mol. Life Sci.* **66**, 3685–3695 (2009).
63. H. Kajiura *et al.*, Two *Eucommia* farnesyl diphosphate synthases exhibit distinct enzymatic properties leading to end product preferences. *Biochimie* **139**, 95–106 (2017).
64. A. Hemmerlin, S. B. Rivera, H. K. Erickson, C. D. Poulter, Enzymes encoded by the farnesyl diphosphate synthase gene family in the big sagebrush *Artemisia tridentata* ssp. spiciformis. *J. Biol. Chem.* **278**, 32132–32140 (2003).
65. C.Conart *et al.*, *RNA*-Seq of 10 rose accessions. *NCBI BioProject*. https://www.ncbi.nlm.nih.gov/bioproject/PRJNA911487/. Deposited 13 December 2022.
66. C.Conart *et al.*, Rose RNA-Seq during flower development. *NCBI BioProject*. https://www.ncbi.nlm.nih.gov/bioproject/PRJNA911454/. Deposited 13 December 2022.